Multi-fidelity, steady-state aeroelastic modelling of a 22-megawatt wind turbine

Zahle, Frederik; Li, Ang; Lønbæk, Kenneth; Sørensen, Niels N.; Riva, Riccardo

Published in:
The Science of Making Torque from Wind (TORQUE 2024): Aerodynamics, aeroleasticity, and aeroacustics

Link to article, DOI:
10.1088/1742-6596/2767/2/022065

Publication date:
2024

Document Version
Publisher's PDF, also known as Version of record

Multi-fidelity, steady-state aeroelastic modelling of a 22-megawatt wind turbine

Journal of Physics: Conference Series **2767** (2024) 022065 doi:10.1088/1742-6596/2767/2/022065

Multi-fidelity, steady-state aeroelastic modelling of a 22-megawatt wind turbine

Frederik Zahle, Ang Li, Kenneth Lønbæk, Niels N. Sørensen, Riccardo Riva

Department of Wind and Energy Systems, Technical University of Denmark, Roskilde, DK-4000, Denmark

E-mail: frza@dtu.dk

Abstract. In this work we present multi-fidelity steady-state aeroelastic framework that leverages the state-of-the-art simulation tool HAWC2 for the structural model, and a variety of aerodynamic models, comprising of the low fidelity blade element momentum (BEM) method, the medium fidelity blade element vortex cylinder (BEVC) method and the coupled near wake and vortex cylinder method, and finally the high-fidelity CFD solver EllipSys3D. The aeroelastic framework is part of AESOpt, an aerostructural framework for design of wind turbine blades. The different aerodynamic models are applied to compute the aeroelastic steady state of the newly designed IEA 22 MW Reference Wind Turbine. The results show a very good agreement between the medium- and high-fidelity aerodynamic models with a maximum of 2.7% difference between the high-fidelity aeroelastic response and that of the lower fidelities.

1 Introduction

Both land-based and offshore wind turbines are increasingly being designed using advanced aeroelastic tailoring resulting in large deflections and torsion in order to reduce mass of the blades and to reduce loads on the turbine platform overall. The increased flexibility leads to a more complex aeroelastic response of such structures, and typically also leads to turbines with smaller margins of aeroelastic stability. Therefore, there is a continuing need to improve and validate the numerical methods used to model the aero-elastic response of such turbines, to reduce the risks of failure of the turbines once operating in the field. State-of-the-art nonlinear elastic beam and multi-body modelling has shown to be efficient and accurate for the structural modelling, and the blade element momentum (BEM) method [1] is the main working horse for wind turbine aerodynamic modelling, for both steady-state calculations and time-domain unsteady simulations. The BEM method is an engineering aerodynamic model, which couples the blade element theory (BET) for the inner 2-D airfoil problem and the momentum theory (MT) for the outer 3-D wake problem. Despite it being the industry standard and having surprisingly good agreement when predicting the integral rotor loads, the BEM method is strictly only applicable to straight blades forming a planar rotor [2]. This is because the influence of the blade curved geometry on the wake geometry and consequently on the inductions and the loads are not modelled. This provides challenges when using the BEM method for design optimization and load calculation of blades with large deflections and also novel tip designs with curved shapes [3, 4]. There have been many recent developments on the corrections and extensions to further extend the BEM method to model blade sweep effects [5, 6, 7, 8] and blade dihedral [2, 9] on the loads. These advanced engineering aerodynamic models are referred to as medium-fidelity models, since the influence of wake

geometry on the loads is modelled in a physically consistent manner. To assess detailed aerodynamic performance and verify the medium-fidelity models, high-fidelity aerodynamic modelling is, however, also needed. This could for example be to assess the performance of novel tip shapes or enhancement of the performance of thick aerofoils used on the inner part of the blade, or design of add-on solutions such as vortex generators and root spoilers. Traditionally, CFD-based evaluation of the rotor performance has been carried out considering only the aerodynamics. However, to correctly predict the power performance of a rotor, fully coupled aero-elastic modelling is needed for modern rotors, which is usually referred to as fluid structural interaction (FSI). Several works exist that carry out FSI simulations on wind turbine rotors, some with application to operational cases [10, 11] and others focusing on complex off-design standstill cases [12, 13], and generally focus on time domain simulations. To make 3D CFD-based FSI tractable in a design context, in which blade design candidates are continuously assessed, the FSI solution process should ideally not incur computational overhead relative to a standard steady-state CFD solution. A commonly used approach has been to apply the deformations predicted by a medium-fidelity aeroelastic code to the CFD mesh in a preprocessing step, which will often be reasonably accurate, but will crucially not capture the change in deformations from possibly different aerodynamic response from the CFD solver.

In this work, we present a multi-fidelity steady-state aeroelastic framework that couples the beam finite element multi-body code HAWC2 with a suite of steady-state aerodynamic solvers. Aerodynamic solvers with different fidelities can be chosen, from the low-fidelity BEM method to the mid-fidelity advanced engineering aerodynamic models and to the high-fidelity computational fluid dynamics (CFD) solver EllipSys3D [14, 15, 16]. The aero-elastic coupling is part of a larger, fully parameterized, aerostructural design framework, which allows us to vary both the internal structural geometry and the aerodynamic shape, and compute the updated structural properties used in the aero-elastic solution procedure. This allows us to effectively explore design variations and carry out numerical shape optimization leveraging the multi-fidelity, multi-disciplinary library of tools in the framework. This part of the framework is, however, not the focus of this paper.

This manuscript is organized as follows. Sec. 2 describes the tools used for this study. Sec. 3 describes the 22 MW turbine studied in this work. Sec. 4 discusses the solution methodology for the multi-fidelity aeroelastic steady-state solver, and presents the comparison between the high- and medium-fidelity aeroelastic solutions. Finally, in Sec. 5 we draw the conclusions, and provide perspectives for future applications of the framework.

2 Tools

The modelling framework used in this work consists of several core analysis tools, both aerodynamic and structural, as well as an overall framework that handles the external inputs and outputs, couples the analysis tools together, interfaces with numerical optimizers, and includes linear and nonlinear system solvers. Each element of this framework is described below.

2.1 EllipSys3D

EllipSys3D [14, 15, 16] is an incompressible CFD solver developed at DTU Wind and Energy Systems, which has been used and verified across a wide range of application areas. The solver is block-structured and solves the incompressible Navier-Stokes equations using a SIMPLE-like method, in both time domain and steady-state. Several turbulence and transition models are available, and in this work we use the $k-\omega$-SST turbulence model by Menter [17] and the e^n transition model by Drela and Giles [18]. For volume meshing, the in-house hyperbolic mesher HypGrid3D is used [16].

2.2 BEVC

The Blade Element Vortex Cylinder (BEVC) code is a multi-fidelity engineering aerodynamic solver for steady-state load calculations, which is planned to become open source. The fundamental difference compared to the aerodynamic modules implemented in HAWC2 is the steady-state assumption in the BEVC code. The rotor is assumed to be isotropic. That is, it operates under uniform inflow with no wind shear, yaw error or rotor tilt, and therefore all blades have the same loads. In comparison, the BEM module in HAWC2 [1] employs a polar grid approach and is enhanced with various correction models for time-domain simulations of the rotor in turbulent inflow. The definition of the blade planform follows that in HAWC2, which is based on a main axis that is defined to be the half-chord

line[1]. The airfoils are aligned perpendicular to this main axis and the crossflow principle [19] is applied. The aerodynamic models with different fidelities in BEVC will be described in the following, in order of increasing fidelity.

The low-fidelity BEM method is implemented following that in HAWC2 [1]. Prandtl's tip-loss correction is applied to the axial induction to take into account the effect of finite number of blades. The current implementation has two major differences compared to the one in HAWC2: only the lift force is included in the momentum balancing; and the relationship between the axial induction factor a and the local thrust coefficient C_t has two options, either the polynomial relationship by Madsen et al. [1], or the classical relationship with empirical correction for heavily loaded conditions. For blade optimization, the HAWC2 polynomial has been observed to lead to designs with a higher thrust compared to the analytical optimal thrust coefficient of 8/9 that derives from the momentum theory. The blade element vortex cylinder (BEVC) method [2] was developed to model the impact of the wake geometry of prebent blades or coned rotors on the inductions and consequently on the loads. The trailed wake of the rotor is modelled using the superposition of concentric vortex cylinders [20]. The starting position of the vortex cylinder follows the curved surface swept by the blades. For a non-planar rotor, the vortex cylinders are shifted in the streamwise directions and the corresponding impacts on the axial and radial inductions are modelled. In addition, the magnitude and direction of the lift and drag forces should be carefully evaluated [9]. It was shown that this effect is important when modelling non-planar rotors, for all models that use 2-D airfoil data. In a previous work [2], it was shown that the BEVC method has significantly improved agreement with fully-resolved CFD results, compared to the BEM method. The BEVC method still relies on the empirical tip-loss correction, which was derived for straight blades, and it therefore does not predict the effect of blade sweep effect correctly. To this end, it has been shown that both the bound vortex and the trailed vortex should be sufficiently modelled [5]. For a swept blade, the bound vortex is assumed to follow the quarter-chord line, which will be curved. In addition, the trailed vortices will start from this curved bound vortex line, which will be shifted azimuthally in the rotor plane compared to a straight blade. If only the trailed vortex is modelled and the bound vortex influence neglected, there will be an overestimation of the gain in aerodynamic torque when sweeping the blade backwards. The physically consistent method to include the bound vortex influence on itself is shown in [6]. In addition, a large effort was spent to enable the calculation of the trailed wake induction to be computationally efficient [7]. This is because using direct numerical integration of the Biot-Savart law is relatively computationally heavy. A method based on analytical solutions for special flow conditions and corrections for general flow conditions was employed [7]. The computational effort is low and is in similar magnitudes as that of the BEM method and BEVC method. This computationally efficient curved bound vortex and trailed vortex modelling method is labeled as NW. With the NW method coupled with the vortex cylinder model, it is possible to model general curved blades with both sweep and prebend or rotor coning combined. This coupled model is labelled as NW-VC.

Compared to the aerodynamic modules in HAWC2, the current steady-state implementation has some advantages, which makes it suitable for design optimization. First, the steady-state implementation does not rely on time stepping to reach an aeroelastic steady-state as in a time domain simulation tool, such as HAWC2. This makes the steady-state computation very fast. Second, compared to HAWCStab2 with the aerodynamic module and structure module inherently coupled, the code has much greater flexibility. This makes it possible to apply aerodynamic models with different fidelities. Third, the code can compute analytical gradients of its outputs with respect to typical design variables such as blade geometry and airfoil data in both forward and reverse (adjoint) modes using algorithmic differentiation (AD). Compared to the finite differencing (FD) method, the gradients are calculated with low computational effort and are machine-accurate.

2.3 HAWC2 static solver

HAWC2 [21] is a wind turbine dynamic simulator. Structural members are modelled via Timoshenko beam elements, where the stiffness matrix can either be uncoupled or fully populated. The latter option allows modelling modern blades with composite materials and possibly bend-twist coupling. Nonlinear deflections and rotations are modelled via the floating-frame of reference formulation. In Ref. [22] it was shown how having as many bodies, i.e. floating reference frames, as elements provides the most accurate structural response. The associated increase in computational cost is contained by employing the sparse Newmark, or static, solver. Several types of constraints, implemented with the Lagrange multipliers method, allow modelling arbitrary topologies.

[1] It is future work to make the definition general, which is beneficial to represent a larger design space of the 3D blade geometry.

This work leverages a newly developed static solver, which computes the nonlinear static solution for an arbitrary distribution of external, in this case aerodynamic and centrifugal, loads. The blades collective pitch angle and rotor speed are constant during the static solution, and provided externally. The static solver iteratively updates the sparse stiffness matrix, computes the external loads and solves a linear system to determine the increment for the structural degrees of freedom.

2.4 AESOpt

The wind turbine aerostructural optimization framework AESOpt [23] enables fully coupled aerostructural design of wind turbine blades, allowing simultaneous optimization of the internal structural and outer aerodynamic geometry of a blade. It has interfaces to the cross-sectional finite element code BECAS [24], HAWC2 for the structural modelling, HAWCStab2 [25] for the aeroelastic stability analysis, the multi-fidelity engineering rotor aerodynamics code BEVC, as well as to the CFD code EllipSys3D. Aerostructural optimization workflows currently primarily use low- to medium-fidelity aerodynamic modelling, but the CFD code EllipSys3D has previously been used to optimize blade tips using both surrogate-based and direct gradient-based methods [26, 3]. The framework uses the WindIO wind turbine ontology developed in the IEA Wind Task 37 [27] to represent the turbine inputs. Based on WindIO, the turbine geometry is parameterized related to e.g. blade planform and internal structural geometry. The overall aerostructural framework is implemented in OpenMDAO [28]. In this work, we focus on the implementation and application of the nonlinear static FSI solution procedure, which can be solved using various schemes using standard API interfaces in OpenMDAO, for which details are presented in Section 4.1. The FSI coupling is implemented based on Python-wrapped shared library versions of HAWC2 and EllipSys3D. HAWC2 internally handles the interpolation of the aerodynamic loads onto the structure in a conservative manner. On the aerodynamic side, the individual blade surface grid points are associated with specific span-wise beam positions through a mapping typically generated at the time of surface grid generation. When the beam deforms, its deflections and rotations are enforced at the surface grid points through the mapping, and the deformation is pushed into the volume grid through a quaternion based mesh deformation method blending along surface normal grid lines. This procedure is identical to what is used in the existing time-domain coupling between HAWC2 and EllipSys3D [10, 13].

3 The IEA 22 MW Reference Wind Turbine

The IEA 22 MW reference wind turbine (RWT) [29, 30] is a recently published open-source reference turbine that was designed collaboratively between DTU and NREL in the context of IEA Wind Task 55 [31]. The rotor diameter is 284 m, with a hub height of 170 m, it has a direct-drive generator, and the turbine features both a monopile and a semi-submersible floating platform. DTU led the design of the rotor, for which AESOpt was used, while NREL designed the hub, drivetrain, monopile and semi-submersible floater. The rotor uses the FFA-W3 airfoil family along the span of the blade, as well as interpolated and manually generated flatback airfoils for relative thicknesses between 48% and 90% on the inner part of the blade. The lofted blade shape is shown in Figure 1. Airfoil data for the turbine were computed with EllipSys2D for Reynolds numbers representative for normal operating conditions, ranging between 8×10^6 and 18×10^6, both with wall surface modelling assuming fully turbulent flow using the k-ω-SST model, as well as modelling taking into account laminar to turbulent transition using the Drela-Giles model. The default airfoil dataset for aeroelastic computations is one with a mix of turbulent and free-transition conditions in the ratio 30/70%, but for this study we use the pure turbulent and free-transition polars to enable direct comparison to 3D CFD computations with the same turbulence and transition modelling.

3.1 Model Setup

The CFD surface mesh used in the present work was generated using the in-house surface mesh generator PGL [32] and resolves the blade surface with 256 cells in the chordwise direction, and 128 cells in the spanwise direction. The volume mesh was generated with HypGrid3D and had a so-called O-O spherical topology, and had 128 cells normal to the surface with a first cell height of $2{\times}10^{-6}$ m. All three blades are included in the mesh, resulting in a total of 14×10^6 cells in the mesh.
The BEVC models and the HAWC2 beam model resolve the blade with 40 nodes (and 39 bodies in HAWC2). When extracting spanwise loads from the CFD solver, the same distribution of nodes is used for consistency.

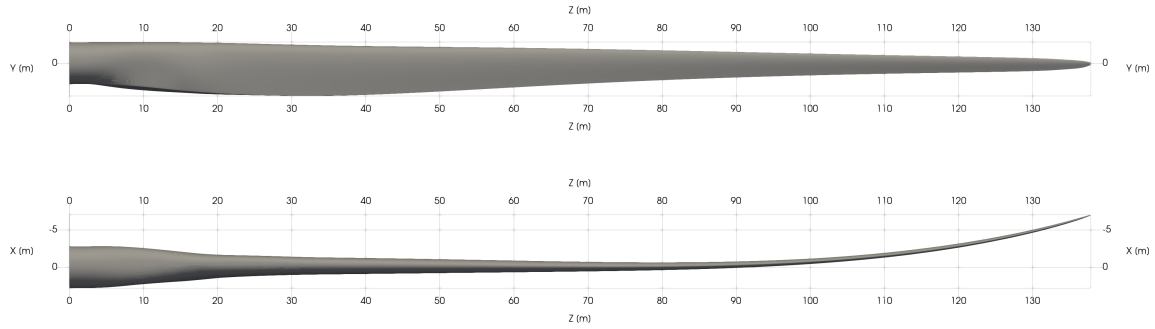

Figure 1: Top- and side-view of the IEA 22 MW RWT blade. Reproduced from [29].

4 Results

4.1 Coupled aeroelastic steady-state

The static aero-elastic solution is solved using an iterative fixed-point Nonlinear Block Gauss-Seidel (NLBGS) scheme, that iterates between the structural and aerodynamic solvers until the change in their respective solutions are below a chosen threshold, which is applied to both the low- to mid-fidelity and high-fidelity aerodynamic models. Since the low- to mid-fidelity aerodynamic models are computationally very fast, they are solved to full convergence at every coupling iteration. However, since the CFD solver has a significantly higher computational cost in the coupling, we do not converge the CFD solver fully between each coupling iteration. Instead, a fixed number of CFD iterations are run in each FSI iteration, where 400 iterations was found suitable for EllipSys3D. To accelerate further the coupling, we initialize the solution procedure on a coarse grid representation on the CFD side to establish an approximate deformed shape before converging the FSI problem further on the fine grid. This solution strategy is standard practice for the solver, and not something developed for the present FSI solution scheme. As a result, the FSI scheme only adds negligible computational overhead compared to a standard steady-state CFD computation. Figure 2 shows the convergence history of the NLBGS solver overlaid with the flow solver momentum residual. As can be observed, for the present case, the flow solver reaches a limit cycle at around 6000 iterations, which is due to the flow not reaching a steady-state in the root part of the blade. The numerical noise in the forces affects the convergence of the FSI solution, which consequently also reaches a limit cycle and fails to converge fully. Although numerically not converged, the changes in deflections and forces are negligible for engineering analysis; this is illustrated in the right plot in 2, where in fact the deflected shape has visually converged already on the coarser grid (after 2000 CFD iterations). Dicholkar et al [33] recently demonstrated that the so-called modified BoostConv method is capable of stabilising steady-state CFD solvers for a wide range of problems, and application of this method to the flow solver would allow us to converge the problem numerically. This is, however, beyond the scope of the present work. The computations were deemed converged after 20 Gauss-Seidel iterations, which on DTU's Sophia cluster [34] required about 1.3-1.5 hours of walltime on 216 cores. For comparison, the medium fidelity NW-VC model converges in 2.3 s (including the framework overhead) for a single wind speed, with approximately 10 NLBGS iterations converged to 8 orders of magnitude accuracy across all wind speeds.

4.2 Multi-fidelity comparison

In this section, the aeroelastic steady-state response across a range of wind speeds for different aerodynamic models is presented. The four levels of aerodynamic fidelities are labelled as follows: *CFD* for the highest fidelity, where both turbulent (*-tu*) and transitional (*-tr*) computations were made; For the low- to mid-fidelity modelling, the BEM method is labelled as *BEM*; the blade element vortex cylinder labelled *BEVC*; and finally the coupled near wake and vortex cylinder model is labelled as *NW-VC*. For these modelling fidelities two sets of airfoil data were used: turbulent (*-tu*) and transitional (*-tr*) 2D CFD based data.

Figure 3 shows the rotor power and thrust across a range of wind speeds, as well as the power and

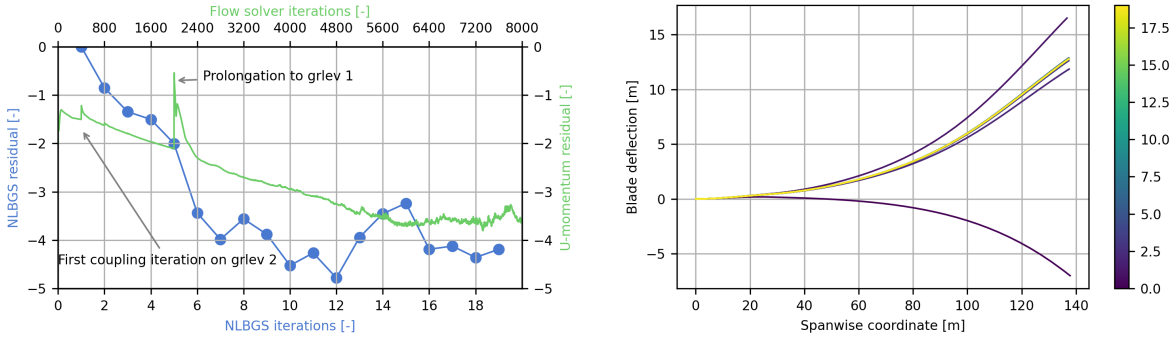

Figure 2: Left, convergence history of the nonlinear aeroelastic solution and the flow solver, right, blade flapwise deflection for each NLBGS iteration. Arrows indicate the first coupling iteration on the coarsest grid (grlev 2), as well as the point at which the solver prolongs to the fine grid level (grlev 1).

	Power [kW]			Thrust [kN]		
WSP [m/s]	CFD-tr	BEVC-tr	Diff. [%]	CFD-tr	BEVC-tr	Diff. [%]
6.0	4.359e+03	4.240e+03	-2.741	1.174e+03	1.150e+03	-2.076
8.0	1.027e+04	9.996e+03	-2.662	2.071e+03	2.019e+03	-2.535
10.0	1.886e+04	1.851e+04	-1.890	2.765e+03	2.693e+03	-2.600
12.0	2.379e+04	2.364e+04	-0.6328	2.557e+03	2.507e+03	-1.929

Table 1: Rotor power and thrust for the aeroelastic solutions based on CFD considering transitional flow (CFD-tr) and one using the BEVC method (BEVC-tr). The percentage difference is computed as the relative difference of the medium-fidelity models to the CFD results.

thrust coefficients, comparing the 3D CFD aeroelastic solutions with the BEVC solutions. Table 1 lists the power and thrust for the transitional computations, along with relative differences between the two fidelities. Overall, we observe a good agreement between the mid- and high-fidelity models, where it is found that the high-fidelity model predicts higher power and thrust of maximum 2.7% and 2.6%, respectively. For brevity, the turbulent results are not included in the table, but similar differences are observed.

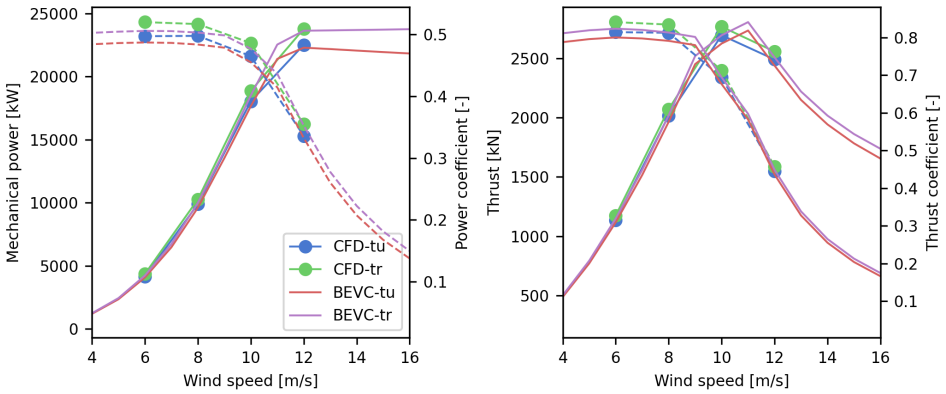

Figure 3: Rotor power and power coefficient (left), and rotor thrust and thrust coefficient (right), comparing the aeroelastic solution based on CFD with one using the BEVC method.

Figures 4 shows a more detailed comparison between the four modelling fidelities for spanwise quantities local power and thrust coefficients, as well as flapwise deflections and torsional deformations in Figure 5. There is an overall trend where the CFD results show higher loading towards the inner- and mid-span of the blade, while at the tip lower loading than the mid-fidelity models. This trend is also more clearly visible in the plots of the difference between the CFD and mid-fidelity results, shown only for the 10 m/s case in Figure 6. The predicted flapwise deflections are in excellent agreement across the fidelities with only 0.3 m or 1.5% difference for the 10 m/s case, which has the highest deflection. At this wind speed, the blade has significant torsional deformation with approximately 5° torsion at the blade tip. For the torsional deformation, we observe again very good agreement between the fidelities with a slightly higher relative difference of 4% at 10 m/s. There is a consistent offset in flapwise deformation between the medium-fidelity and high fidelity results on the inner 60 m of the blade, for which the CFD-based results show a higher positive deflection. We attribute these discrepancies to be due to differences in predicted aerodynamic loading on the inner part of the blade, where the medium fidelity codes rely on interpolated 2D airfoil data, which in the current results does not consider 3D effects. Further investigations are, however, needed to ascertain this conclusion.
In general, as shown in Figure 4, the aeroelastic steady-state predicted by the three low- to mid-fidelity models are similar. The impact of different model fidelities is very little. The performance of the highest-fidelity in this category, which is the NW-VC method, does not have significant improvements compared to the lowest-fidelity BEM method. For a wind speed of 10 m/s, the results in Figure 6 show that the BEVC method has the best performance when predicting the flapwise and torsional deformations, which is improved compared to both BEM and NW-VC. Further investigations are necessary to discover the reason that the NW-VC method is not performing better than BEVC when predicting blade deflections. When comparing the predicted local power and thrust coefficient, the performance of the models with different fidelities is as expected. The results from the NW-VC method have the best agreement with the CFD results while the BEM method has the worst performance.

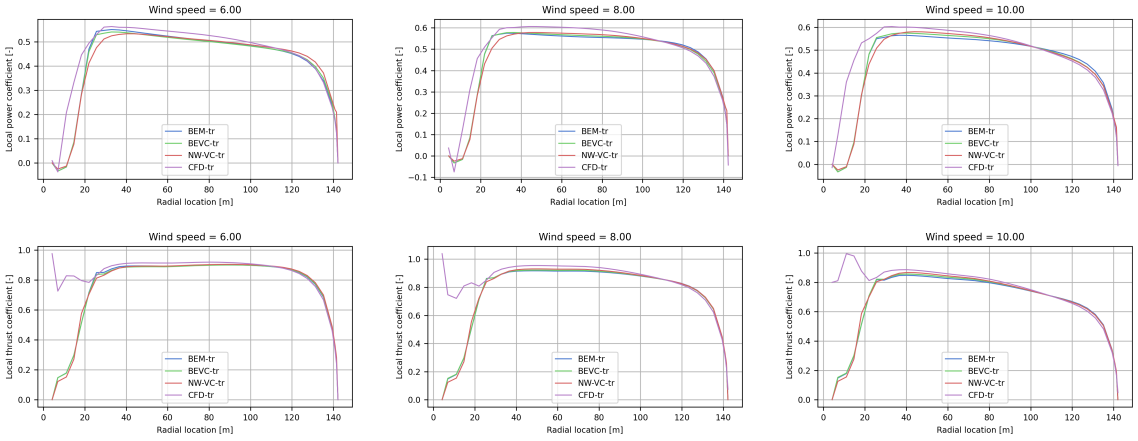

Figure 4: Local power and thrust coefficients across the four modelling fidelities. All models assume free transition (*-tr*).

The generally very good agreement across the modelling fidelities presented in this work can on the one hand be attributed to the high accuracy of the BEVC code, and consistent implementation of the aeroelastic coupling. But it is also important to mention that for comparisons between blade resolved CFD with aerodynamic models based on look-up airfoil data, consistency of the airfoil data and the 3D CFD method should be considered a prerequisite for achieving consistent results. Although good agreement is observed in the present work because the airfoil data used is based on same CFD solver as used for the 3D computations, further improvement could be expected from the use of airfoil data based directly on 3D CFD.
Although we did not observe significant differences between the basic BEM method and the BEVC and BEVC-NW methods, we expect to observe more significant differences for more advanced tip shapes that incorporate significant amounts of prebend and sweep. It is beyond the scope of the present work to demonstrate this and will be the subject of future research.

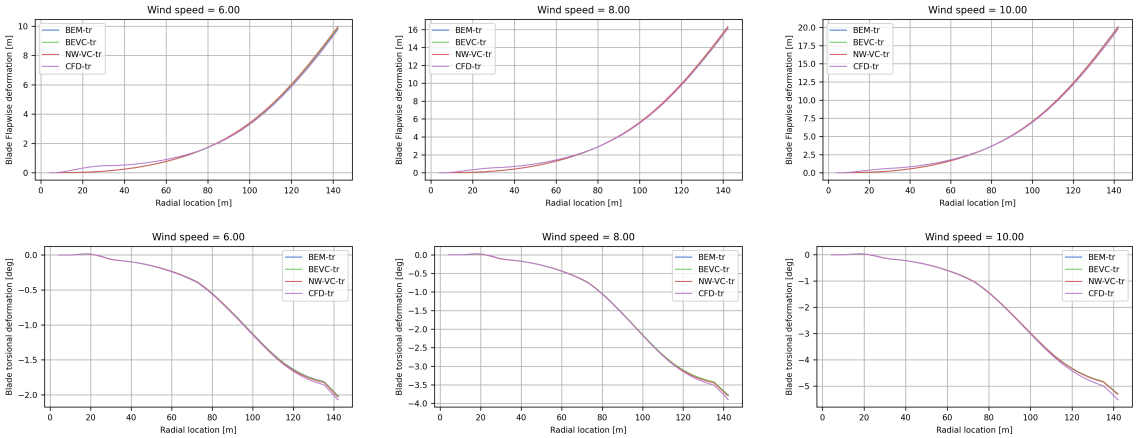

Figure 5: Flapwise and torsional deformations across the four modelling fidelities. All models assume free transition (*-tr*).

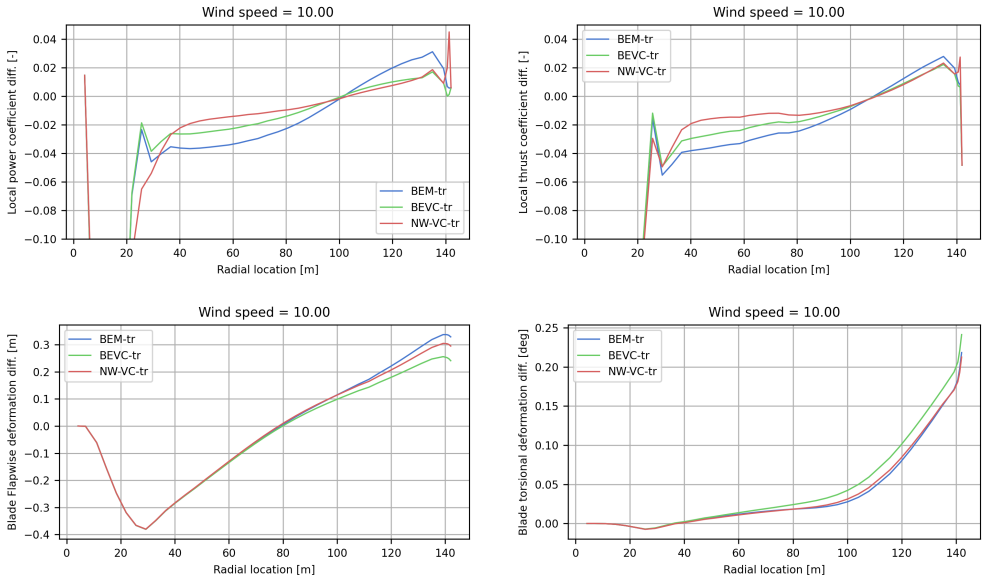

Figure 6: Difference in local power and thrust coefficients, flapwise deflection and torsional deflection between the aero-elastic solution based on EllipSys3D and low- to mid-fidelity methods, including BEM, BEVC and NW-VC, computed at 10 m/s wind speed.

5 Conclusions

In this work a multi-fidelity framework for aeroelastic steady-state analysis has been presented, which is part of the aerostructural design tool AESOpt. The framework leverages the multibody beam code HAWC2 for the structural modelling, and the multi-fidelity aerodynamics code BEVC and the CFD solver EllipSys3D to model the aerodynamics. The framework leverages OpenMDAO to solve the nonlinear aeroelastic problem using the Nonlinear Block Gauss-Seidel solver implemented in OpenMDAO. Details on the solution strategy for the FSI solver was presented in which the flow and aeroelastic solution are converged simultaneously, resulting in negligible overhead of solving aeroelastically compared to a pure aerodynamic solution due also to the negligible cost of the structural solver.

The framework was applied to aeroelastic analysis of the IEA 22 MW RWT, for which very good

agreement across the four modelled aerodynamic fidelities was found. The present results demonstrate that the medium-fidelity aerodynamic modelling used in AESOpt for design optimization of the IEA 22 MW RWT is indeed of high accuracy compared to high-fidelity CFD modelling, providing a solid basis for aerostructural design of wind turbine rotors. The tightly integrated multi-fidelity modelling framework provides very interesting perspectives related to design optimization and exploration of advanced blade shapes. For example, in Zahle et al. [26, 3], advanced tips were designed using both surrogate-based and direct optimization techniques. Extension of these works to consider the aeroelastic response of the blade can now be achieved and also greatly accelerated using well-established multifidelity optimization techniques, where the medium-fidelity BEVC-NW model can be used.

Acknowledgements
This work has been supported partially by the AMTip project, funded by the Energy Technology Development and Demonstration Programme (EUDP) (Case no. 64021-2062). All computations have been carried out on the DTU Sophia cluster [34].

References

[1] Madsen H A, Larsen T J, Pirrung G R, Li A and Zahle F 2020 *Wind Energy Science* **5** 1–27

[2] Li A, Gaunaa M, Pirrung G and Horcas S 2022 *Wind Energy Science* **7** 75–104 ISSN 2366-7443

[3] Madsen M, Zahle F, Horcas S, Barlas T and Sørensen N 2022 *Wind Energy Science* **7** 1471–1501 ISSN 2366-7443

[4] Horcas S, Ramos-García N, Li A, Pirrung G and Barlas T 2023 *Wind Energy* **26** 5–22 ISSN 1095-4244

[5] Li A, Pirrung G, Madsen H A, Gaunaa M and Zahle F 2018 *Journal of Physics: Conference Series* **1037** ISSN 1742-6596

[6] Li A, Gaunaa M, Pirrung G R, Ramos-García N and Horcas S G 2020 *Journal of Physics: Conference Series* **1618** 052038

[7] Li A, Pirrung G, Gaunaa M, Madsen H and Horcas S 2022 *Wind Energy Science* **7** 129–160 ISSN 2366-7443

[8] Fritz E K, Ferreira C and Boorsma K 2022 *Wind Energy* **25** 1977–1994

[9] Li A, Gaunaa M, Pirrung G, Meyer Forsting A and Horcas S 2022 *Wind Energy Science* **7** 1341–1365 ISSN 2366-7443

[10] Grinderslev C, Sørensen N, Horcas S, Troldborg N and Zahle F 2021 *Wind Energy Science* **6** 627–643 ISSN 2366-7443

[11] Guma G, Bucher P, Letzgus P, Lutz T and Wüchner R 2022 *Wind Energy Science* **7** 1421–1439

[12] Heinz J, Sørensen N, Zahle F and Skrzypinski W 2016 *Wind Energy* **19** 2041–2051 ISSN 1095-4244

[13] Horcas S, Sørensen N, Zahle F, Pirrung G and Barlas T 2022 *Physics of Fluids* **34** ISSN 1070-6631

[14] Michelsen J A 1994 Block structured multigrid solution of 2D and 3D elliptic PDEs Tech. Rep. AFM 94-06 Technical University of Denmark

[15] Sørensen N N 1995 General purpose flow solver applied to flow over hills Tech. Rep. Risø-R-827(EN) Risoe National Laboratory

[16] Sørensen N N 1998 HypGrid2D—a 2-D mesh generator Tech. Rep. Risø-R-1035(EN) Risoe National Laboratory

[17] Menter F R 1993 Zonal two equation kappa-omega turbulence models for aerodynamic flows *23rd Fluid Dynamics, Plasmadynamics, and Lasers Conference*

[18] Drela M and Giles M B 1987 *AIAA Journal* **25** 1347–1355

[19] Hörner S F and Borst H V 1985 *Fluid-dynamic lift: practical information on aerodynamic and hydrodynamic lift* (Textbook published by the author)

[20] Branlard E and Gaunaa M 2015 *Wind Energy* **19** 1307–1323 ISSN 1095-4244

[21] Larsen T J and Hansen A M 2022 How 2 HAWC2, the user's manual Tech. Rep. Risø-R-1597(ver. 4-5)(EN) Risø National Laboratory URL `www.hawc2.dk`

[22] Gözcü O and Verelst D R 2020 *Wind Energy Science* **5** 503–517 ISSN 2366-7451

[23] Zahle F, Lønbæk K, Li A and Riva R 2023 *AESOpt - Aero-Structural Optimization Framework for Wind Turbine Design* version 0.32 URL `https://aesopt.pages.windenergy.dtu.dk/aesopt`

[24] Blasques J P and Stolpe M 2012 *Composite Structures* **94** 3278 – 3289 ISSN 0263-8223

[25] Hansen M 2011 Aeroelastic properties of backward swept blades *49th AIAA Aerospace Sciences Meeting including the New Horizons Forum and Aerospace Exposition* (Reston, Virigina: American Institute of Aeronautics and Astronautics) ISBN 978-1-60086-950-1

[26] Zahle F, Sørensen N, McWilliam M and Barlas A 2018 Computational fluid dynamics-based surrogate optimization of a wind turbine blade tip extension for maximising energy production vol 1037 (IOP Publishing) ISSN 1742-6596

[27] Bortolotti P, Bay C, Barter G, Gaertner E, Dykes K, McWilliam M, Friis-Moller M, Molgaard Pedersen M and Zahle F 2022 System modeling frameworks for wind turbines and plants: Review and requirements specifications Tech. Rep. DOI: 10.2172/1868328 URL `https://www.osti.gov/biblio/1868328`

[28] Gray J S, Hwang J T, Martins J R R A, Moore K T and Naylor B A 2019 *Structural and Multidisciplinary Optimization* In Press

[29] Zahle F, Barlas A, Lønbæk K, Bortolotti P, Zalkind D, Wang L, Labuschagne C, Sethuraman L and Barter G 2024 Definition of the IEA Wind 22-Megawatt Offshore Reference Wind Turbine Tech. Rep. DTU Wind Report E-0243, ISBN 978-87-87335-71-3 DTU Wind and Energy Systems

[30] 2023 https://github.com/ieawindtask37/iea-22.0-280-rwt

[31] 2023 IEA Wind Task 55 - REFWIND – reference wind turbines and plants: https://iea-wind.org/task55/

[32] Zahle F 2020 PGL: parametric geometry library URL `https://gitlab.windenergy.dtu.dk/frza/PGL`

[33] Dicholkar A, Zahle F and Sørensen N 2022 *Journal of Wind Engineering & Industrial Aerodynamics* **220** ISSN 0167-6105

[34] Technical University of Denmark 2019 Sophia HPC cluster URL `https://dtu-sophia.github.io/docs/`